



CHORUS

This is the accepted manuscript made available via CHORUS. The article has been published as:

Alternative search strategies for a BSM resonance fitting the ATLAS diboson excess

Biplob Bhattacharjee, Pritibhajan Byakti, Charanjit K. Khosa, Jayita Lahiri, and Gaurav Mendiratta

Phys. Rev. D **93**, 075015 — Published 6 April 2016

DOI: [10.1103/PhysRevD.93.075015](https://doi.org/10.1103/PhysRevD.93.075015)

Alternative search strategies for a BSM resonance fitting ATLAS diboson excess

Biplob Bhattacharjee^a, Pritibhajan Byakti^b, Charanjit K. Khosa^c,

Jayita Lahiri^d and Gaurav Mendiratta^e

Centre for High Energy Physics, Indian Institute of Science, Bangalore- 560012, India

Abstract

We study an s-channel resonance R as a viable candidate to fit the diboson excess reported by ATLAS. We compute the contribution of the ~ 2 TeV resonance R to semileptonic and leptonic final states at 13 TeV LHC. To explain the absence of an excess in semileptonic channel, we explore the possibility where the particle R decays to additional light scalars X, X or X, Y . Modified analysis strategy has been proposed to study three particle final state of the resonance decay and to identify decay channels of X . Associated production of R with gauge bosons has been studied in detail to identify the production mechanism of R . We construct comprehensive categories for vector and scalar BSM particles which may play the role of particles R, X, Y and find alternate channels to fix the new couplings and search for these particles.

PACS numbers: 13.38.-b, 12.60.-i

^a biplot@cts.iisc.ernet.in

^b prtibhajan@cts.iisc.ernet.in

^c khosacharanjit@cts.iisc.ernet.in

^d jayita@cts.iisc.ernet.in

^e gaurav@cts.iisc.ernet.in

I. INTRODUCTION

Resonant searches in the s-channel mediated $2 \rightarrow 2$ process are special as they can provide a smoking gun signal for beyond standard model (BSM) physics at the LHC. ATLAS collaboration has recently reported a $2.6\sigma - 3.4\sigma$ excess in their searches for BSM resonances in diboson channel decaying into two fat jets final states from 20.3 fb^{-1} of data at 8 TeV LHC run[1]. Any hints in the electro-weak (EW) sector in TeV energy are exciting as almost all the major ultraviolet (UV) completions of the standard model (SM) predict TeV scale particles. The observed diboson invariant mass distribution shows a bump in 1.8-2.2 TeV region. This gives further support to the weak evidence of an excess of $(1\sigma-2\sigma)$ which were already seen in the same channels by the CMS experiment in a similar invariant mass region[2].

Since the excess arises at 2 TeV scale, the final state gauge bosons(W/Z) are highly boosted and collimated. In the hadronic decay of a boosted gauge boson, the light quark jets produced are also highly collimated and form one fat jet (J). While looking for the two fat jet final states whose jet mass lies within 20 GeV range of W/Z mass, ATLAS found the largest discrepancy near 2 TeV corresponding to 3.4σ , 2.6σ and 2.9σ significance in WZ , WW and ZZ channels respectively. Considering entire mass range 1.3-3.0 TeV in each of the search channel, the global significance of the discrepancy in the WZ channel is 2.5σ .

Any BSM particle which decays to two standard model gauge bosons W/Z will also have semileptonic and leptonic final states because of the leptonic decay modes of W and Z . Therefore in addition to the dijet channel, semileptonic channels should also see some excess because of comparable branching. However, no such excess has been observed in the searches by CMS or ATLAS[3–7]. In the combined analysis of hadronic, semileptonic and leptonic final states, ATLAS finds that the largest deviation from the background expectation is 2.5σ and corresponds to a 2 TeV invariant mass[8]. This significance is smaller than the 3.4σ significance observed in the JJ channel as the semileptonic and leptonic channels are consistent with the background-only hypothesis. One should notice that the leptonic branching fraction of W and Z are very small, for example the fully leptonic decay channel, $ZZ \rightarrow 4l$, is not very competitive in the diboson resonance search at 8 TeV.

In other related searches, ATLAS and CMS collaborations have presented their results and put upper limits on the Zh/Wh production cross section[9–11]. CMS collaboration

observes a 2.2σ excess over the standard model at $m_{Wh} \approx 1.8$ TeV in the $l\nu b\bar{b}$ final state[10]. Dijet resonance searches also show a (2.1σ) discrepancy in the invariant mass region of ≈ 2 TeV[12, 13]. Individually these searches have a low statistical significance and may get ruled out with early LHC run II[14]. At the same time, the combination of all of these excesses and the appealing properties of TeV scale BSM physics encourage us to look for more ways to discover BSM physics in the early LHC run II.

Naturally, any hint of a discrepancy between SM predictions and observations creates a renewed excitement and a flurry of suggestions for possible explanations and suggestions for further explorations. The possible models which may explain partly or fully, the above experimental results include additional new gauge bosons such as W' , Z' [15], composite Higgs models[16], heavy Higgs boson(s)[17–19], string originated[20], R -parity conserving[21] or violating[22] supersymmetric models, walking technicolor[23] and other spin one resonances [24]. The effective field theory approach for bosonic resonance production is also used to study diboson channel[25].

In this study we explore comprehensively, the production, decay and coupling measurement of a BSM s-channel scalar or vector bosons which can fit the diboson excess. In section II, we will review all the experimental results from ATLAS and CMS involving the diboson search. We follow the same strategy as adopted by ATLAS to estimate the number of events for WW , WZ and ZZ states decaying to semileptonic and leptonic channels at 13 TeV LHC run. To study BSM models, we start with discussing status of two particle final states coming from the decay of a heavy resonance. In section III, we discuss the possibility of excess only in hadronic decay mode of the gauge bosons at 13 TeV LHC run which might be due to light BSM particle mimicking the W/Z boson signatures at LHC. We explore such a model and find general signatures of its decay modes to isolate the BSM physics. In section IV, we explore the production mechanism of the heavy resonance to look for probes which can distinguish between quark-quark or gluon-gluon initiated processes. We propose alternate channels and cuts to distinguish these two cases in the associated production process. Next we comment on how to independently measure the couplings of the BSM resonance with gauge bosons and quarks. In section V, we check the viability of three particle final state as a possible mimic for the diboson excess. In section VI, we discuss and categorize simplified models which can accommodate a 2 TeV resonance and additional W/Z -like BSM particles with mass ~ 100 GeV. In the last section, we discuss some general experimental signatures

common to many of the proposed BSM simplified models. If LHC run II confirms 2 TeV resonance with greater statistical significance, following the strategy described in our paper, its couplings and decay modes can be identified in the early LHC run.

II. ANALYSIS

ATLAS experiment at LHC has reported diboson excess around 2 TeV in the hadronic decay of gauge bosons only[1]. The updated analysis including the leptonic and semi leptonic final states is also available [8]. Since gauge bosons coming from the heavy resonance will be very boosted, so their decay products will be highly collimated. Two quarks from hadronic decay of W/Z boson will look like a single jet of bigger radius and these objects are called fat jets. ATLAS has scanned the invariant mass range of 1.3 – 3 TeV to look for any BSM resonance decaying to the diboson channel. As the final states are fat jets, in their analysis, jets are constructed using C/A method with radius 1.2. After jet formation, a grooming algorithm, a variant of mass drop technique, is applied to find pair of quarks forming fat jet and to reduce pileup. Mass drop technique is used to examine the sequence of pairwise combinations used to reconstruct the jet in order to find two subjets corresponding to the W or Z boson decay. Feynman diagram for this process is given in Fig.1. For semileptonic and leptonic decay channels, in order to maximize the sensitivity to resonances with different masses, three different optimized set of selection criteria are used according to the p_T of the leptonically ($W(p_T^{\ell\nu})/ Z(p_T^{\ell\ell})$) and hadronically decaying W/Z boson (p_T^{jj} or p_T^J where p_T^J means the p_T of the fat jet)[8]. These three regions are called low p_T resolved, high p_T resolved and merged region. As the resonance is 2 TeV, its decay products will be highly boosted and p_T of boosted objects will be greater than 400 GeV and high p_T merged region is most suitable for this scenario. CMS has not observed any excess in diboson final state. In Table I we quote the CMS 95 % CL upper bound on cross section. We will discuss ATLAS analysis in detail for each channel one by one.

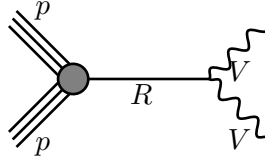


FIG. 1. Feynman diagram for resonance decaying to two vector bosons.

A. Resonance decaying to WW , ZZ or WZ

1. JJ channel

ATLAS has observed the excess in this channel from 2 TeV resonance decay. This channel is sensitive to WW , ZZ and WZ decay modes of the resonance. As discussed earlier from the decay product of the gauge bosons we will get two fat jets. The events with fat jets having subjets less than 3 are considered. Fat jet pair invariant mass is demanded to be greater than 1050 GeV. QCD dijet is the largest background for JJ channel and is reduced by using following cuts

1. Jet mass $m_J \in (82.4 \pm 13/92.8 \pm 13)\text{GeV}$, $|\eta| < 2$ and $\frac{p_T^{J_1} - p_T^{J_2}}{p_T^{J_1} + p_T^{J_2}} < 0.15$ ($p_T^{J_1}$ and $p_T^{J_2}$ denote p_T of first and second jet respectively) to tag W/Z bosons
2. Number of charged tracks < 30 for ungroomed jets to remove higher multiplicity gluons
3. Rapidity difference $|y_1 - y_2| < 1.2$ between 2 leading jets to remove the large t-channel gluon mediated background

In addition to the above cuts, the ATLAS analysis removed events with a prompt electron ($E_T > 20$ GeV, $|\eta| < 1.37$ or $1.52 < |\eta| < 2.47$) or a muon ($p_T > 20$ GeV, $|\eta| < 2.5$) to avoid overlap with leptonic decay searches in diboson channel and also removed events with

$\cancel{E}_T > 350$ GeV to remove overlap with searches with $Z \rightarrow \nu\bar{\nu}$. The 95 % CL upper limit on diboson cross section for all the processes corresponding to 2 TeV resonance from ATLAS are given in Table II.

Upper bound on cross section (in fb)	WW	ZZ	WZ
JJ	16	18	16
$l\nu J$	3.5	–	–
llJ	–	8.5	–
$lll\nu$	–	–	21

TABLE I. CMS 8 TeV, 95 % CL upper limits on diboson cross section ($pp \rightarrow R \rightarrow VV$) for different channels corresponding to 2 TeV resonance[2–4].

Upper bound on cross section (in fb)	WW	ZZ	WZ
JJ	30	30	30
$l\nu J$	5	–	9
llJ	–	8	20
$lll\nu$	–	–	21
Combined (hadronic + leptonic)	13	13	15

TABLE II. ATLAS 8 TeV, 95 % CL upper limits on diboson cross section ($pp \rightarrow R \rightarrow VV$) for different channels corresponding to 2 TeV resonance[1, 8].

2. $l\nu J$ channel

The updated ATLAS analysis of the diboson excess also includes leptonic decays of gauge bosons[8]. One can get $l\nu J$ final state either from WZ or WW decay. Events which have only one isolated (high p_T) lepton fall under this category. Following cuts have been used :

1. Jet invariant mass range : $65 < m_W < 105$ GeV and $70 < m_Z < 110$ GeV

2. Lepton $p_T > 25$ GeV
3. Jet $p_T^J > 400$ GeV
4. $\cancel{E}_T > 30$ GeV
5. $p_T(l\nu) > 400$ GeV (vector sum of p_T vector of \cancel{E}_T and that of lepton)

Main backgrounds in this channel are $W + \text{jet}$, top quark pair production and non-resonant diboson production. The cut $\Delta\phi(\cancel{E}_T, J) > 1$ is applied to reject multi-jet background. Top quark production background is reduced by rejecting the events with b-tagged jet having $\Delta R > 0.8$ (with fat jet).

3. llJ channel

This channel is sensitive to ZZ and WZ final state only. All the cuts for this channel are same as previously discussed channels except the condition of same flavour opposite sign dilepton pair. The invariant mass (m_{ll}) of the lepton pair is required in 65-115 GeV range. Main background processes are $Z + \text{jets}$, top quark pair and non-resonant vector boson pair production.

4. $lll\nu$ channel

Here three isolated leptons each with $p_T > 25$ GeV and $\cancel{E}_T > 25$ GeV are demanded. Out of these leptons, two should be of same flavour and opposite sign. Invariant mass of that pair of leptons should be within 70-110 GeV ($m_Z \pm 20$ GeV) range since they can be produced only from Z decay. One can get this final state only from WZ decay. Dominant backgrounds for this channel are SM- WZ and ZZ production. Data driven method is used to estimate these background processes.

ATLAS has observed an excess in the JJ channel of gauge boson decay. If the resonance is a true signal, beyond statistical fluctuations, the 13 TeV LHC will be able to see a sharp peak in the JJ channel because the cross section will increase significantly at 13 TeV. The JJ channel is sensitive to WW , WZ and ZZ decay modes equally because of same hadronic branching of W and Z boson. Therefore from this channel we can't distinguish whether the resonance is dominantly decaying to WW , WZ or ZZ . Moreover along with the JJ channel

the other decay modes of W and Z i.e. the semileptonic and fully leptonic channels should also observe some clear excess. If the 13 TeV LHC sees some excess events in semileptonic or fully leptonic decay channels, we will be able to distinguish which decay mode of the resonance is preferred. For example, the $ll\nu$ channel is only sensitive to WZ ; $llll$ is sensitive to ZZ only; $l\nu J$ is sensitive to both WW and WZ . But significant events in $l\nu J$ channel, and no event in $ll\nu$ will ensure that the final state is WW . If they observe no signal in any of the channels, they will be able to rule out the possibility that the resonance decays to diboson final state.

Channel	Cuts	No of signal events (5fb^{-1})			No. of background events (5fb^{-1})
		WW	ZZ	WZ	
$l\nu J$	$p_T^l > 25 \text{ GeV}, p_T^J > 800 \text{ GeV}, p_T^{l\nu} > 800 \text{ GeV}$	65		30	20
llJ	$1.8 \text{ TeV} < m_{llJ} < 2.2 \text{ TeV}, p_T^J > 400 \text{ GeV}, p_u^T > 400 \text{ GeV}$		30	10	2
$ll\nu$	$p_T^{l_1} > 100 \text{ GeV}, p_T^{l_2} > 100 \text{ GeV}, p_T^{l_3} > 100 \text{ GeV}$			4	4
$llll$	$p_T^{l_1} > 60 \text{ GeV}, p_T^{l_2} > 60 \text{ GeV}, p_T^{l_3} > 60 \text{ GeV}, p_T^{l_4} > 60\text{GeV}$		1		2

TABLE III. Expected number of events for different leptonic channels at 13 TeV. The S/\sqrt{B} ratio has been optimized to obtain the cuts.

To check this, we have done a detailed analysis following the same strategy as ATLAS to calculate the expected number of events in each channel at the 13 TeV LHC. We have also estimated the major backgrounds for all these channels. We used CalcHEP[26] for parton level event generation, Pythia 6.4.28[27] for showering and fastjet-3.1.3[28] for jet formation. Only track isolation is applied to count the number of isolated leptons. If the p_T sum in cone of radius 0.2 (around the lepton) is less than 15 % of lepton p_T then that lepton is declared as an isolated lepton. For $l\nu J$ channel, we have considered $W + \text{jets}$, $Z + \text{jets}$ and SM VV production process as main backgrounds. In case of llJ , we have considered $Z + \text{jet}$ and SM VV production as backgrounds. In case of $llll$, SM VV have been considered as dominant background. The results are presented in Table III. We have assumed $\sigma(pp$

$\rightarrow R \rightarrow VV) \approx 100$ fb for all WW , ZZ and WZ final states at 13 TeV. In principle these three cross sections can be different from each other but one can rescale the number of events accordingly. The optimized cuts used to reduce the background and to increase the signal significance are also listed in Table III. We have also estimated the 13 TeV signal and background (only QCD dijet) events for the JJ channel, we find that there will be 12 signal events corresponding to 32 background events with 400 GeV p_T cut on fat jets. For accurate background estimation one has to consider the large systematic uncertainty for JJ channel.

We can see from the table that WW channel can be easily differentiated from the other modes with only 5 fb^{-1} of data, because in the WW case, there will be an excess only in the $l\nu J$ channel. To see the events in the fully leptonic channel, we need higher luminosity $\sim 100 \text{ fb}^{-1}$. In case we find some excess in llJ channel but not in $l\nu J$ channel that will definitely correspond to ZZ final state. If one finds excess in both $l\nu J$ and llJ channel then it will be the WZ final state.

III. RESONANCE DECAYING TO TWO BSM PARTICLES

In the previous section we have discussed the expected number of events in all the leptonic final states of WZ , WW and ZZ decay channels at the 13 TeV LHC. Observation of these events will confirm that a resonance actually decays into a pair of gauge bosons. If we do not see any excess in the semileptonic and leptonic decay channels of gauge boson at 13 TeV and the hadronic signature of BSM survives, it would rule out the models where the resonance decays to W/Z bosons dominantly. In such a case, an additional particle X (see Fig.2) with a mass in 70-100 GeV range which decays to light quarks/gluons will be required to explain this excess. The possible decays of particle X are discussed below,

1. It can decay to light quarks or gluons.
2. One can get $b\bar{b}$ final state from X decay. In this case, with b-tagging of the fat jets one will be able to identify this final state. Although the b-tagging efficiency will be less for high p_T jets ($< 50\%$)[29], but still it is possible to count number of b-subjets inside fat jets.
3. The particle X can also decay into pair of τ leptons. This decay mode can not be

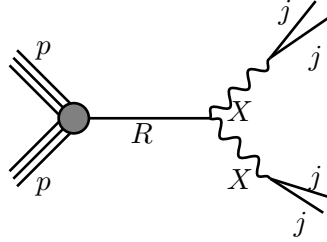


FIG. 2. Feynman diagram for resonance decaying to pair of particle X .

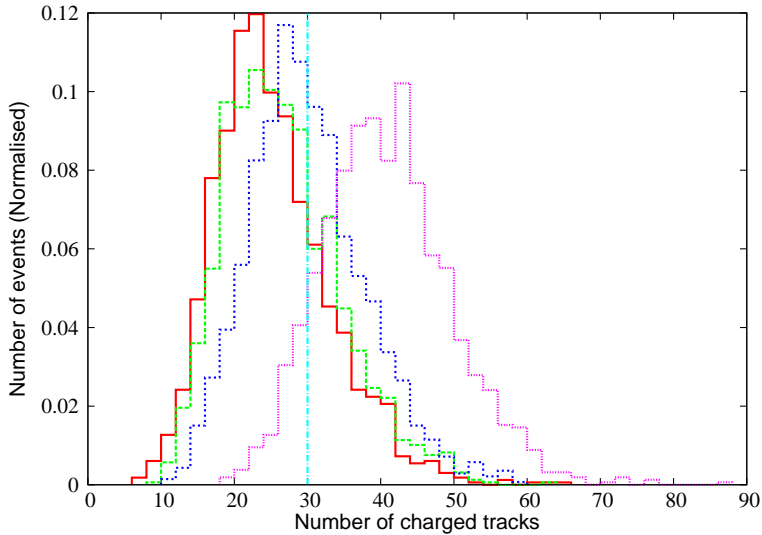


FIG. 3. Normalized charge multiplicity distribution for highest p_T jet formed by different ($u\bar{u}$ - red, $c\bar{c}$ - green, $b\bar{b}$ - blue and $g\bar{g}$ - violet) decay modes of particle X .

dominant decay channel of X otherwise we will see some excess in the leptonic channels of diboson searches through tau decay. We can observe ditau tagged (boosted) fat jets and identify this final state also.

We have studied in detail different scenarios, where X can decay into gluons or quarks. Using Pythia 6.4.28, tune (AUET-2B) and pdf-CTEQ6L1, we have simulated the listed decay channels of the particle X . In Fig.3, we show number of charge tracks in the fatjet

with $p_T > 540$ GeV coming from $u\bar{u}$, $c\bar{c}$, $b\bar{b}$ and gluon-gluon final states for comparison. If it decays to gluons then one finds more number of charge tracks in a fat jet as compared to quark jets[30]. As the ATLAS analysis is based on a number of charge tracks (inside a fat jet) cut (< 30), the gluon final state should not be the dominant decay mode of X to avoid reduction in the cross section via the branching fraction. Additionally, with the experimental cuts, signal selection efficiency in case of gluon jets is very small (20 %) and we need high cross section to observe this final state. It is very difficult to distinguish $u\bar{u}$, $c\bar{c}$ and $b\bar{b}$ final states from charge track distribution unless the b-jets are tagged. As mentioned earlier, in the high p_T regions, b-tagging efficiency is lower. Once we have enough data, we can see b-subjets in the fat jets. When one X decays to quarks and the other to gluons, this scenario can be identified within low luminosity because quark-quark final state has more signal selection efficiency, as shown in the Fig.3.

The particle X can be tracked via its decay modes discussed above at early LHC run-II. The gluon fraction in the final state can be checked by changing (increasing) the number of charge track cut on the fat jet. For dijet final state the QCD background also becomes large when this cut is relaxed. But associated dijet production scenario which will be discussed in the next section may form a viable channel for the final state analysis, because of less background.

IV. ASSOCIATED RESONANCE PRODUCTION

Having discussed the 13 TeV projections of the various leptonic decay modes of the newly observed resonance, we expect that the LHC run II can easily see the resonance through these channels also, and can identify its decay modes precisely. Then one will have clear understanding of decay modes of the 2 TeV resonance. Our next task is to address the issue of production mechanism of this state. Question arises whether the production of the resonance R is a quark initiated or a gluon initiated process. Quarks have tree level gauge couplings with electroweak gauge bosons but these couplings do not exist for gluons. Therefore for quark initiated process we can get gauge bosons W^\pm , Z , γ and g (see Fig.4 for Feynman diagrams) emission from the initial quark legs. Associated production of R with W, Z, γ will ensure that the initial state involves quarks. Gluons have tree level couplings with quarks as well as self coupling. Hence a gluon jet can come from both quark or gluon

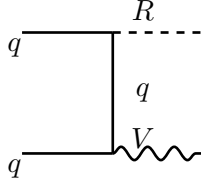


FIG. 4. Feynman diagram for the quark initiated RV production process.

leg in the initial state (see Fig.5(a)), therefore associated gluon production with R can not distinguish the initial states¹. But if gluon coupling with R exists we will also get associated quark jet with R from the process depicted in Fig.5(b). Using quark/ gluon tagging it may be possible to verify the existence of the process depicted in Fig.5(b) along with the processes shown in Figs.5(a), (c) and (d). This will then confirm that the resonance is produced through gluon fusion. On the other hand, as W^\pm , Z , γ can only come from quark initiated process, any signature of the associated production of R with W^\pm , Z and γ will ensure that R is produced through quark coupling. Schematic of associated production is as follows :

$$qq \rightarrow RV \rightarrow WW + W/Z/\gamma \rightarrow JJ + l\nu/ll/\gamma \quad ; \quad qq \rightarrow R \rightarrow WW \quad (1)$$

Typical signals one should look for RW and RZ production at 13 TeV LHC are $JJl\nu$ and JJl^+l^- .

From this discussion it is evident that associated production of RV is an important channel to explore at the 13 TeV LHC. Hence we will estimate the cross section for this process. For that one has to specify the model. There have been many analyses based upon spin 0, spin 1 and spin 2 resonance, to explain diboson excess. We consider in our work, a spin 0 resonance, produced through quark initiated process. Having spin information we

¹ In [31] associated jet production channel has been considered where the resonance decays invisibly.

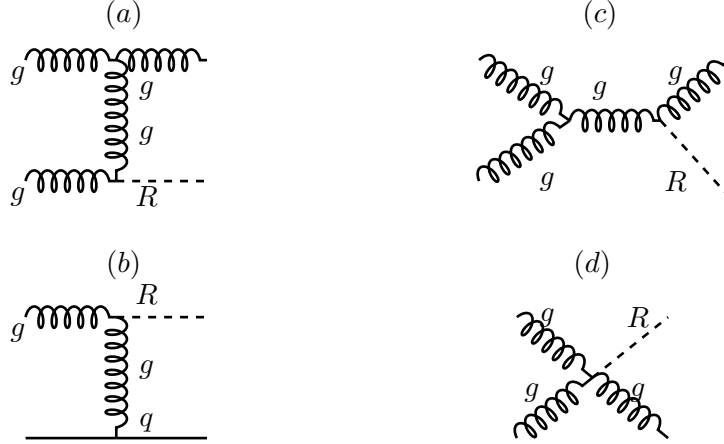


FIG. 5. Feynman diagrams for associated production of R with jets.

can find out the viable model parameter space in context of the reported excess. We assume R is a scalar having Higgs like couplings and it couples to only light quarks and massive gauge bosons at tree level. The cross section of the process ($pp \rightarrow R \rightarrow VV$) involves only two couplings, the coupling C_{Rqq} which is the Yukawa type coupling between R and the light quarks (u and d) and C_{RVV} coupling between R and gauge bosons. In our case the $C_{RWW/RZZ}$ coupling is SM $C_{hWW}^{SM}/C_{hZZ}^{SM}$ coupling scaled by a free parameter. The scaling parameter is same for both the couplings. The C_{hWW}^{SM} and C_{hZZ}^{SM} couplings are $\frac{eM_W}{\sin\theta_W}$ and $\frac{eM_W}{\sin\theta_W \cos^2\theta_W}$ respectively. The coupling C_{Rqq} also determines the dijet cross section. From the dijet resonance searches by ATLAS and CMS at 8 TeV, $\sigma(pp \rightarrow R \rightarrow jj) < 100$ fb for a 2 TeV resonance[12, 13]. Our aim is to look for parameter space consistent with both diboson and dijet constraints. We find that to satisfy dijet cross section limit $C_{Rqq} < 0.33$. As mentioned earlier the process $pp \rightarrow R \rightarrow VV$ involves both C_{Rqq} and C_{RVV} coupling and its cross section is proportional to product of these two couplings. In Fig.6 we show $\sigma(pp \rightarrow R \rightarrow VV)$ contours in the C_{Rqq} and C_{RVV} plane. The whole parameter space shown in Fig.6 is compatible with the 8 TeV dijet constraints[12, 13]. The maroon dotted line denotes the contour which gives the diboson $\sigma(pp \rightarrow R \rightarrow VV) \approx 10$ fb which is the

upper limit on the diboson cross section from ATLAS. So parameter space below this curve is allowed by the diboson search. We have plotted the projected limit for 14 TeV LHC for the dijet cross section[32]. The red solid line in Fig.6 is the projected dijet limit for 14 TeV. Only the region to the left of this line will be allowed by the dijet search at 14 TeV. Assuming Z'_B model, 14 TeV limits on Z' -quark coupling has been calculated in [32]. Using this limit, we have calculated 14 TeV projected limit on dijet cross section which we used to extract the 14 TeV limit on the C_{Rqq} coupling in our model, corresponding to 300 fb^{-1} luminosity. We can see from the figure that 14 TeV LHC can rule out most of the currently allowed parameter space. We have considered only the four decay modes, $R \rightarrow u\bar{u}, d\bar{d}, WW, ZZ$ of the resonance R . For each point of the parameter space spanned by C_{Rqq} and C_{RVV} considered in the Fig.6, we have calculated decay width of R dynamically using CalcHEP. Throughout the parameter space allowed by the diboson and dijet constraints i.e. the region below the contour of 10 fb cross section, the width of R is below 10% of the mass of R . Hence it can be considered as a narrow width. In the regions where the cross-section is beyond 10 fb, the width of the resonance R can be greater than 10 % of its mass. In that region the narrow width approximation will not be valid. Therefore that region will be generally excluded by the experiment.

We have chosen few benchmark points (C_{Rqq}, C_{RVV}) from the allowed parameter space. In Table IV we quote the 13 TeV associated RV , dijet and associated dijet cross section for the benchmark points.

Our objective is to present a projection of the associated production of R with gauge bosons for 13 TeV LHC. Using first benchmark ($C_{Rqq} = 0.3, C_{RVV} = 2.67$) point we have generated 20,000 parton level events for $pp \rightarrow RW$ and RZ processes, using CalcHEP. We pass these events to Pythia 6.4.28 for hadronization and used fastjet for jet formation. Main backgrounds for these processes are $W/Z + \text{jets}$. To ensure that the lepton(s) coming from W/Z are isolated and well separated from the decay products of the high p_T gauge bosons, we plot ΔR distribution between W and R in Fig.7 (a). The W boson p_T distribution for associated RW is given in Fig.7 (b). One can see from these two figures that the lepton will be indeed isolated and it will carry enough p_T such that this can be a clear signal to identify at LHC. We estimate the number of events for $JJl\nu$ and $JJll$ processes for 13 TeV LHC run. All our cuts are same as JJ channel of ATLAS diboson analysis except for the JJ invariant mass cut which we consider in the range 1.8-2.2 TeV in this case. Diboson

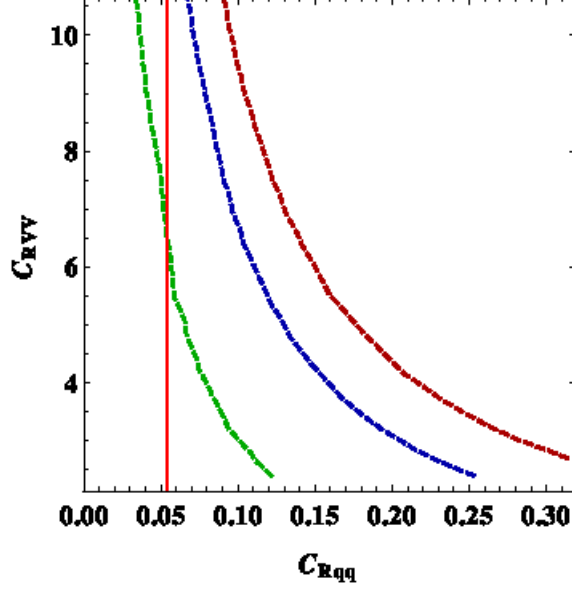


FIG. 6. Contours of constant $\sigma(pp \rightarrow R \rightarrow WW)$ (fb) in C_{Rqq} C_{RVV} plane. The maroon, blue and green dotted curves denote 10 fb, 5 fb and 1 fb cross section contours respectively. The red solid line is the projected dijet bound at 14 TeV.

C_{Rqq}, C_{RVV}	(0.3, 2.67)	(0.09, 10.13)	(0.11, 7.99)
$\sigma(RW)$	75.6 fb	6.8 fb	10.26 fb
$\sigma(RZ)$	32.4 fb	3.02 fb	4.42 fb
$\sigma(R\gamma)$	4.24 fb ($p_T > 20$ GeV)	0.72 fb ($p_T > 20$ GeV)	1.14 fb ($p_T > 20$ GeV)
$\sigma(\text{dijet})$	470.0 fb	1.44 fb	4.8 fb
$\sigma(\text{associated dijet})$	57.6 fb	0.16 fb	0.6 fb

TABLE IV. 13 TeV cross section estimate for different processes for three benchmark points.

signal strength will be maximum in the narrow region around 2 TeV. For associated RW production in the $JJl\nu$ final state we have used the following cuts :

1. $30 < p_T^l < 350$ GeV
2. $30 < E_T < 350$ GeV

For associated RZ decaying to $JJll$ final state only the lepton p_T cut is used. Expected number of events for $JJl\nu$ and $JJll$ are given in Table V and VI respectively.

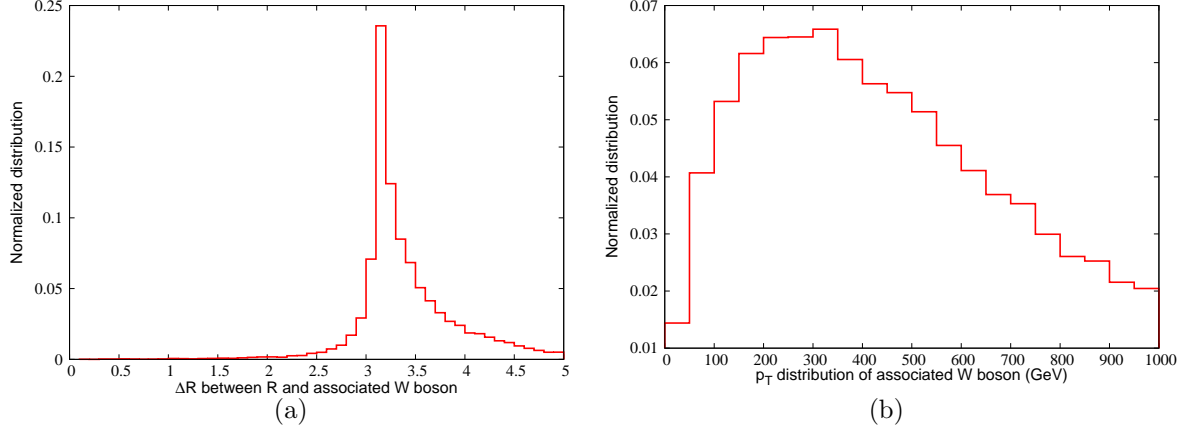


FIG. 7. (a) Distribution of ΔR between R and W , (b) p_T distribution of W produced in association with R .

\sqrt{s}	8TeV	13TeV
Total No. of Generated Events	20000	20000
$\sigma(pp \rightarrow RW)$	5 fb	75.6 fb
$JJl\nu$	277	161

TABLE V. Expected number of events for $JJl\nu$ from RW associated production for couplings $C_{Rqq}=0.3$ and $C_{RVV}=2.67$.

If the resonance is produced through quark initiated process then 13 TeV LHC will be able to confirm that looking at associated production of R with gauge bosons in the 2 fat jets +1 lepton + E_T in case of associated RW and a pair of leptons with 2 fat jets in case of associated Z production. The RW final state has maximum cross section, since branching ratio of W to leptons is much higher than Z branching ratio to leptons. The backgrounds

\sqrt{s}	8TeV	13TeV
Total No. of Generated Events	20000	20000
$\sigma(pp \rightarrow RZ)$	2.2 fb	32.0 fb
$JJll$	101	69

TABLE VI. Expected number of events for $JJll$ from RZ associated production for couplings $C_{Rqq}=0.3$ and $C_{RVV}=2.67$.

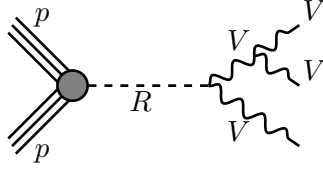


FIG. 8. Feynman diagram for three vector bosons final state.

for these processes are found to be negligible.

Although we have argued that looking at associated production of R with gauge bosons is the best strategy to identify the production mechanism of R , we should also mention that a $2 \rightarrow 3$ process where R decays to WWZ (s-channel diagram - see Fig.8) will give us the same signature as the associated production RZ (where $R(\rightarrow WW)Z$) or RW ($(R \rightarrow WZ)W$). This process can be originated from quark-quark or gluon-gluon initial states. These two cases can be distinguished from various kinematic distributions. For example, in case of the s-channel diagram (see Fig.8) the vector boson emitted from the final state will be highly energetic as it is coming from the decay of a 2 TeV resonance. This will not be the case when the vector boson is emitted from the initial quark leg (see Fig.4). Moreover, the typical cross section for this type of processes is 0.5 fb and 4 fb approximately at 8 TeV and 13 TeV respectively for the first benchmark point ($C_{qqR}=0.3$ and $C_{RVV}=2.67$). We can see from Table IV that the cross section of this process is much smaller than the typical RW or RZ associated production cross section. There is another way to distinguish between these two cases. In addition to looking for leptonic signals with two fat jets, one should also count the number of positive and negative charged leptons in this process. We will always find some asymmetry in the lepton number count if it is a quark initiated process. The reason behind this is that the cross section of $u\bar{d} \rightarrow RW^+$ and $d\bar{u} \rightarrow RW^-$ is different in proton-proton collider. Absence of total lepton charge asymmetry will reflect the possibility that we

are looking at three gauge boson final state, produced through R decay, through s-channel production of R (see Fig.8). Hence looking at the associated production of R with W as well as counting the number of positive and negatively charged leptons one can be definite about the production process of R . The s-channel production of RW or RZ which also has the same final state as the associated production is not important, because its cross section is of the order of 10^{-5} fb.

As one of our objective is to extract the couplings C_{Rqq} and C_{RVV} , we have looked at two other processes which involve such couplings. Diboson production gives an upper bound on the product of C_{Rqq} and C_{RVV} as discussed earlier. We have given dijet and associated dijet ($pp \rightarrow RV \rightarrow jjV$) production cross section for a few benchmark points. These two processes depend only on the C_{Rqq} coupling and if we can extract this coupling from their cross section we will be able to comment on C_{RVV} coupling. We should comment here that the dijet production process has large QCD background. Hence coupling measurement from this channel has a lot of uncertainty. Associated dijet production is contaminated with less background. Hence this channel is better to extract couplings.

V. STATUS OF THREE PARTICLE FINAL STATE

So far we have considered $2 \rightarrow 2$ topology. Recently it has been argued in [33] that resonance (which we denote by R) can also decay to three particles in the final state as shown in Fig.9. The schematics of this type of process is $pp \rightarrow V_1V_2X$. We generate parton level events for R decaying to 3 body final state. For this process we have three new particles : X , Y and R , including the resonance. We explore the possibility of this final state mimicking the diboson final state. The particle X can decay into visible or to invisible final states. There is no excess in the leptonic and semileptonic decay channels, hence we assume X can not decay to charged leptons. In case X decays invisibly, there will be a p_T asymmetry between the visible final states. Hence we calculate the fraction of events respecting jet p_T asymmetry cuts for different combinations of Y and X particle masses. We have taken a few benchmark points for X and Y masses. We have explicitly put the invariant mass cut of $1.8 \text{ TeV} < m_{V_1V_2} < 2.2 \text{ TeV}$ on the visible final state particles. We can see from the Table VII that it is very difficult to satisfy p_T asymmetry condition unless X is very light. For $M_X=10 \text{ GeV}$, only 29 % of the events pass the p_T asymmetry cut. But even if this is the

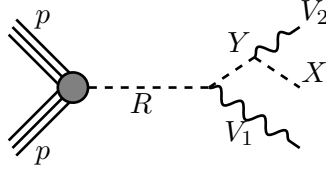


FIG. 9. Feynman diagram for resonance decaying to two vector bosons and a BSM particle.

M_Y (GeV)	M_X (GeV)	Fraction of events with $p_T^A < .15$
150.0	10.0	0.29
200.0	50.0	0.15
300.0	50.0	0.15
300.0	100.0	0.06
400.0	200.0	0.00

TABLE VII. Fraction of events passing p_T asymmetry $\left(p_T^A = \left(\frac{p_T^{V_1} - p_T^{V_2}}{p_T^{V_1} + p_T^{V_2}} \right) \right)$ and invariant mass ($1.8 < m_{V_1 V_2} < 2.2$ TeV) cut when X decays invisibly.

case, one can confirm this decay chain by looking at the two fat jets + E_T signal. In Fig.10 we show the E_T distribution at 13 TeV.

Second possibility is when X decays to hadronic final states. Again we look for fraction of events when X lies within ($\Delta R < 1.2$) fat jet radius (see Fig.11). We can see from the Table VIII that most of events will pass this condition. Even with high X mass 86 % of the events will have X and V_2 (W or Z) lying within fat jet radius. In that case, the invariant mass of the two fat jets will also peak around 2 TeV. But still there is a way to

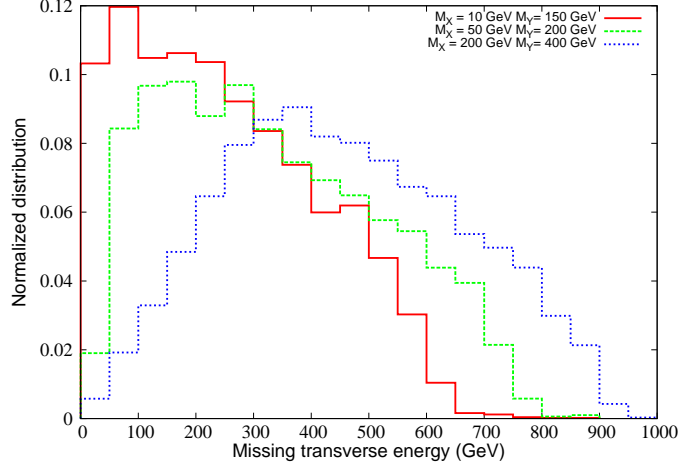


FIG. 10. Distribution of \cancel{E}_T from invisible X decay for three different sets of X and Y masses as shown in the inset.

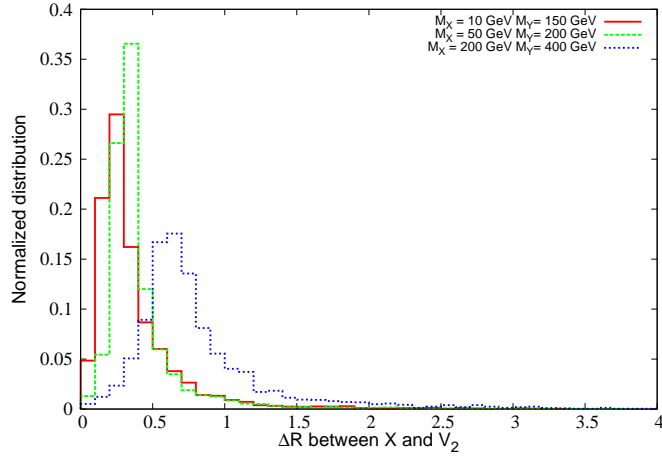


FIG. 11. Distribution of ΔR between X and V_2 for three different sets of X and Y masses as shown in the inset.

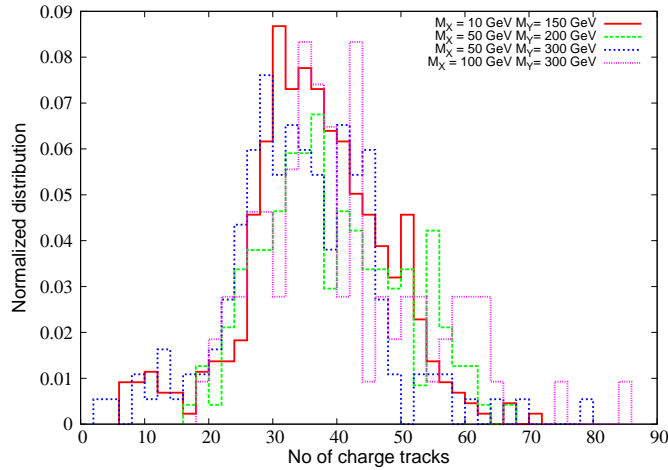


FIG. 12. Normalized charge multiplicity distribution for highest p_T jet for three benchmark points.

M_Y (GeV)	M_X (GeV)	Fraction of the events with $\Delta R_{XV_2} < 1.2$
150.0	10.0	0.97
200.0	50.0	0.97
300.0	50.0	0.86
300.0	100.0	0.91
400.0	200.0	0.86

TABLE VIII. Fraction of events having X decay products within fat jet radius, for different values of Y and X mass.

rule out this possibility. One of the fat jet invariant mass will peak at M_Y instead of gauge boson mass. Even with low X mass (≈ 10 GeV) only 4 % of the total events pass this criteria. In that case X will be within 1.2 radius and p_T asymmetry cut will also not be able to rule out this possibility. But in that case, the jet substructure inside the fat jet will be different. To identify this scenario one has to slightly modify the mass drop technique to look for two parents instead of one and to identify the jet substructure fully when some of the components are not very massive. There can be another possibility that the X lies outside the 1.2 radius and decays into visible particles. But that probability is only about 10%. So we do not consider that possibility. So if X decays invisibly then low mass X can pass p_T asymmetry cut used by ATLAS and in that case one should look for two fat jets + \cancel{E}_T signal. For visible X decay, ungroomed jet mass will be equal to M_Y . Therefore one will find more substructure, and more number of tracks inside the fat jet. In that case one should follow different strategy to look for jet substructure. We have presented the normalized distribution of number of charge tracks inside a fat jet for $2 \rightarrow 3$ topology in Fig.12 for three sets of values of M_X and M_Y for the cases where X is within the fat jet radius.

We have also considered another possible three particle final state as shown in Fig.13. This case is slightly different from the $2 \rightarrow 3$ process discussed above. Here we consider a four point vertex which is allowed by various models. This process has not been explored in the context of diboson excess. We are exploring the possibility of this final state mimicking the diboson excess. We consider both visible and invisible decay of the proposed BSM

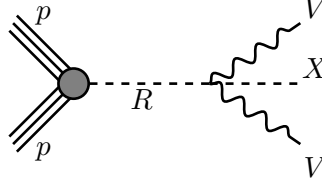


FIG. 13. Feynman diagram for three body resonance decay having two vector bosons and one BSM particle in the final state.

M_X (GeV)	Fraction of events with $p_T^A < .15$
10.0	0.16
50.0	0.14
80.0	0.11
100.0	.10
120.0	.08
150.0	.05
200.0	.02

TABLE IX. Fraction of events passing p_T asymmetry $\left(p_T^A = \left(\frac{p_T^{V_1} - p_T^{V_2}}{p_T^{V_1} + p_T^{V_2}}\right)\right)$ and invariant mass ($1.8 < m_{V_1 V_2} < 2.2$ TeV) cut when X decays invisibly for the diagram shown in the Fig.13.

particle X which we assume to be a scalar.

In case X decays into invisible final states we consider the parton level process $pp \rightarrow R \rightarrow WWX$, $pp \rightarrow R \rightarrow ZZX$ or $pp \rightarrow R \rightarrow WZX$ and look at the p_T asymmetry between the two vector bosons. We present our results in Table IX for few benchmark X mass values.

M_X (GeV)	Fraction of the events with $\Delta R < 1.2$
10.0	29.0
50.0	27.0
80.0	28.7
100.0	27.8
120.0	27.3
150.0	27.4
200.0	26.4

TABLE X. Fraction of events having X decay products within fat jet radius for different values of X mass.

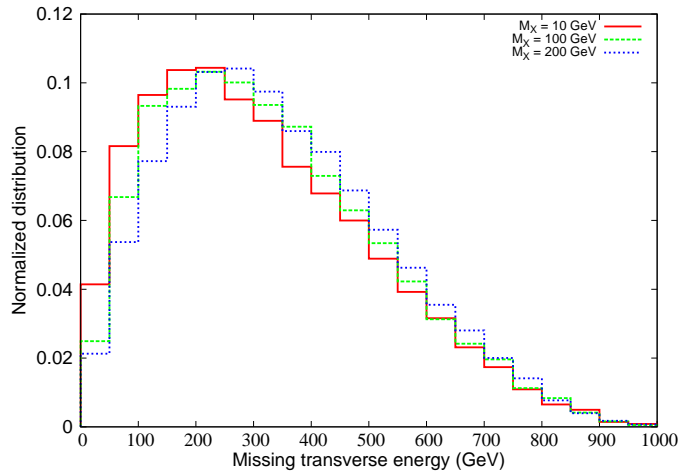


FIG. 14. Distribution of \cancel{E}_T when X decays invisibly for three different sets of X masses as shown in the inset.

We see from Table IX that at most 16 % events can pass the p_T asymmetry condition (along with invariant mass cut : $1.8 \text{ TeV} < M_{VV} < 2.2 \text{ TeV}$) only when X is very light, $M_X \approx 10 \text{ GeV}$. In case of heavy X only 2% events pass this criteria. In case sufficient number of events pass this criteria we should also see some events in the channel $pp \rightarrow 2 \text{ fat jets} + \cancel{E}_T$. We present the \cancel{E}_T distribution for this process in Fig.14.

Next we consider the case where X decays into visible particles. We can safely assume that X can decay into hadronic final states only because otherwise there will be a clear

excess in the final state with more number of leptons. In Table X we show the fraction of events where ΔR between X and one of the gauge bosons is less than 1.2 for all the benchmark points. We can see that for all values of X mass, the number of events for which ΔR is less than 1.2 varies from 26 % to 29% of total number of events. So this final state is not very troublesome. Also in principle one can of course rule out this possibility by looking at the number of the charge tracks of the fat jets. Because in case the X particle is within the fatjet, then the number of charge tracks for that fat jet will be much higher than W or Z fat jet.

Although the final state depicted in Fig.13 is a plausible candidate to mimic the diboson excess, but it is not favoured at all. As we explained above if X decays into invisible final states, the p_T asymmetry cut, the invariant mass cut and \cancel{E}_T cut will reduce the cross section drastically. In case of the visible decay of X a cut on the number of charge tracks inside a fat jet, will reduce the cross section by a factor of 3. Hence the cross section of the process $pp \rightarrow R \rightarrow VVX$ should be much higher than the cross section of the diboson process if diboson excess is misidentification of this process. In addition to that we should also see events in the semileptonic and fully leptonic final states due to presence of gauge bosons in the final states.

VI. ANATOMY OF MODELS EXPLAINING DIBOSON EXCESS

In order to fit the bump observed in the data, s-channel models are favored. In the following section, we will explore a number of viable s-channel BSM models and discuss them in the context of diboson excess and associated processes at LHC.

While building s-channel models, we limit to a two and three body final states. Because, a larger number of particles in the final state would suppress the cross section due to phase space factors and kinematic cuts, for example, p_T asymmetry is required to be less than 15%^[1]. Hence, three topologies exist which can mimic the excess in the diboson data as shown in Fig.15.

In all the considered models, a 2 TeV particle (R) is produced through either a quark initiated or a gluon initiated process². The mediating particle R can be a scalar, vector or

² There can be a quark and gluon (qg) initiated process where R will be a fermion. But this process will be suppressed since the Rqg coupling will be proportional to the ratio of the light and heavy quark mass, so we have not studied this scenario.

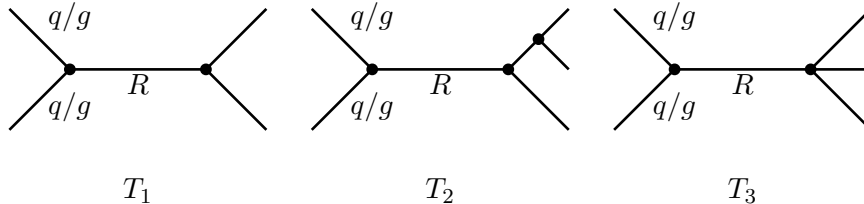


FIG. 15. Possible topologies of s-channel BSM resonance for two and three body final states.

a spin 2 boson³. Next, we discuss the production of the particle R with a gluon or quark initiated state.

A. Production

The resonance R can interact with quarks via tree level couplings whereas with gluons via a 5 or 6 dimensional effective operators. Below, we discuss both of these possibilities in detail.

Gluon initiated process: Here the particle R is produced from gluon fusion. The Kronecker product 8×8 of the color representations of gluon initial state dictates that the particle R can belong to a 1, 8, 10, $\overline{10}$ or 27 dimensional representation of $SU(3)$ [34]. Firstly, we consider the possibility that R is a vector boson. The gluon clearly will not satisfy the role of R since it is massless. On the other hand, single production of any massive gauge boson (R) is not possible from gluon fusion as Landau-Yang theorem forbids it. Thus R cannot be a gauge boson in gluon initiated process.

Next, we consider the case where R is a scalar field. From the point of view of production of a scalar R , all the color representations mentioned above are allowed. As we will see later, the required final state will rule out all the colored representations of a scalar particle R . This leaves, for a color-singlet scalar, two choices of effective interactions with the gluon,

³ We are not considering this possibility in our work.

1. $G_{\mu\nu}G^{\mu\nu}R$,
2. $G_{\mu\nu}G^{\mu\nu}R^\dagger R$.

In the first case, R is a singlet under SM gauge group. In the second case R may have non-trivial representations under $SU(2) \times U(1)$. However, in this case, R has to get a non zero vacuum expectation value (VEV) to obtain a ggR vertex. In addition, tree-level corrections to the ρ -parameter constrains R to belong to one of the $1(1,1,0)$, $2(1,2,\pm\frac{1}{2})$ or $7(1,7,\pm 2)$ dimensional representation of $SU(2) \times U(1)$ [35].

Quark initiated process: If R is a vector gauge boson, the SM gauge group has to be extended with additional symmetries. In principle, a UV completion of SM can be complicated. Though, at the TeV scale, BSM gauge particles interacting with quarks have similar signatures as W' or Z' models. These possibilities have been amply explored in the literature and we limit to the alternative where R is a scalar. For a scalar R , possibilities for its couplings with the quarks are listed in Table XI. Here, we list up to dimension six operators along with the corresponding SM gauge representation of R denoted as $(SU(3), SU(2), U(1))$. The hypercharge listed in the Table XI is defined in a convention where Higgs boson has hypercharge $-\frac{1}{2}$.

B. Explicit models for $2 \rightarrow 2$ topology

After the discussion of production processes, it is now obvious to discuss the decay processes separately and finally discuss the models. However, unlike the production processes, decay processes are different for different topologies. So, to keep our discussion brief we merge analysis of the decay of the resonance R into that of the models.

The decay products of R can be SM EW gauge bosons or BSM particles of similar mass as W/Z bosons. We call the class of models where the final state particles are SM EW gauge bosons W/Z as RVV models. R may decay into WW , ZZ and WZ final states. This class contains some of the minimal extensions of the SM. We arrive at another possibility when one of the outgoing particles is Z or W and other particle is a BSM particle denoted as $R VX$ models. Remaining two possibilities arise when both the decay products of R are BSM particles, denoted as RXX and RXY models, where, in the latter case the two final state particles are different.

Operator	Representation of R
Renormalizable interactions	
$Q_L^T C Q_L R$	$(\bar{6}, 3, \frac{1}{3}), (\bar{6}, 1, \frac{1}{3}), (3, 3, \frac{1}{3}), (3, 1, \frac{1}{3})$
$u_R^T C u_R R$	$(6, \bar{3}, -\frac{4}{3}), (6, 1, -\frac{4}{3}), (\bar{3}, 3, -\frac{4}{3}), (\bar{3}, 1, -\frac{4}{3})$
$d_R^T C d_R R$	$(6, \bar{3}, \frac{2}{3}), (6, 1, \frac{2}{3}), (\bar{3}, 3, \frac{2}{3}), (\bar{3}, 1, \frac{2}{3})$
$\bar{Q}_L u_R R$	$(8, 2, -\frac{1}{2}), (1, 2, -\frac{1}{2})$
$\bar{Q}_L d_R R$	$(8, 2, \frac{1}{2}), (1, 2, \frac{1}{2})$
Higher dimensional	
$(\bar{Q} u_R \tilde{H}) R, (\bar{Q} d_R H) R$	$(8, 1, 0), (1, 1, 0)$
$(\bar{Q} u_R \tilde{H}) R^\dagger R, (\bar{Q} d_R H) R^\dagger R$	$(1, 1, 0), (1, 7, \pm 2)$
$(\bar{Q} u_R H) R$	$(8, 3, -1), (8, 1, -1), (1, 3, -1), (1, 1, -1)$
$(\bar{Q} d_R \tilde{H}) R$	$(8, 3, 1), (8, 1, 1), (1, 3, 1), (1, 1, 1)$
$\bar{q} \not{D} q R$	$(1, 1, 0)$
$\bar{q} \not{D} q R^\dagger R$	$(1, 1, 0), (1, 7, \pm 2)$

TABLE XI. Quark couplings with a scalar particle R . Here the unitary matrix C is charge conjugation matrix. Here Q_L , u_R and d_R are left-handed quark doublet, right-handed up quark and right-handed down quark respectively, q denotes the set $\{Q_L, u_R, d_R\}$. Higgs doublet field is denoted by H with hypercharge $-\frac{1}{2}$.

The final state particles X and Y decay into quarks and mimic the massive vector boson decay products. The particles X and Y may also decay to gluons via effective couplings and may be searched for in this channel. These events are excluded in the diboson analyses due to cuts on number of charged tracks in a jet. Again, in order to pass the experimental cuts for diboson channel, the masses of the additional final state particles X and Y range from 69.4 to 104.8 GeV. This also implies that they cannot be colored particles due to dijet constraints. Though the Table XI is for production processes, we can obtain all the operators, upto dimension six, for X and Y decaying into light quarks just replacing R with X and Y . One can easily readout the possible representations of X and Y from the Table XI. These are listed in the Table XII.

Type of fields	Representation
Singlet	$(1, 1, 0), (1, 1, \pm 1)$
$SU(2)$ doublet like Higgs	$(1, 2, \pm 1)$
$SU(2)$ triplets	$(1, 3, \pm 1)$
The seven dimensional field	$(1, 7, \pm 2)$.

TABLE XII. Possible representations for the choices of scalar R , X and Y . Note that all the representations are colorless.

1. RVV models

The resonant particle R must be a colorless particle as the W and Z bosons do not carry any color. There are only three such possibilities for scalar R : singlet, Higgs-like $SU(2)$ doublet and a seven dimensional representation $(1, 7, \pm 2)$. The collider signature of a vector boson R is similar to either W' or Z' type models.

A weak and color singlet scalar R can be produced through both quark and gluon initiated processes[17]. For a gluon initiated process R must be electrically neutral. An electrically neutral scalar singlet R can decay to WW and/or ZZ through mixing of R with CP even Higgs (h) or through the following higher dimensional operators,

$$W_{\mu\nu}^a W_a^{\mu\nu} R, B_{\mu\nu} B^{\mu\nu} R, \quad (2)$$

where $a = 1, 2, 3$.

For the case where R is a Higgs like doublet, both the quark and gluon initiated production of R are possible[15, 17, 19]. In addition, the two Higgs doublet models (2HDM) also fits, via the charged heavy Higgs, an excess in the search for resonances in W^+h channel[18].

The third possibility where R is an $SU(2)$ seven dimensional scalar is very distinct as it contains exotic fields with charges $\pm 5, \pm 4, \pm 3, \pm 2, \pm 1$ along with the neutral R .

2. RVX , RXX and RXY models

The advantage of introducing non-minimal extensions of SM to explain the observed diboson excess is that the constraints that apply from fully leptonic and semileptonic channels can be partially or fully evaded with non-universal couplings of quarks or leptons with

the BSM particles. We had already discussed why the final state particles are colorless. As W, Z, X and Y are all non-colored, R must also be colorless in all the models. RXX models, even though exotic, allow an explanation for why the experiments see an excess in the fully hadronic final state of the diboson channel and not in the semileptonic and fully leptonic final states.

Next, considering the case where R is a scalar particle which interacts with the quarks. There are 4 possibilities as shown in Table XII. We are going to discuss them one by one.

Singlet scalar R : In a model of type RVX , X can be a singlet, doublet or 7 dimensional representation of $SU(2)$. Upon symmetry breaking, mixing between neutral scalar bosons allows the $R \rightarrow VX$ final state. Similarly, through trilinear couplings arising from the scalar potential after electroweak symmetry breaking, RXX and RXY type models can also be formulated.

$SU(2)$ doublet R : When R belongs to an EW doublet, RVX type models can be formulated, where the final state particle X can belong to any of the four representations listed in Table XII. Since X has a mass similar to the W/Z boson it's multiplet will contain a light charged scalar which will be constrained by $b \rightarrow s\gamma$ [36] process. These constraints can be evaded with large quartic couplings and mass splittings within the X multiplet after symmetry breaking. When X is a singlet, a small mixing with Higgs implies that the coupling of RWX is small and R needs a larger coupling with quarks/gluon to match the required production cross section. RXX and RXY type models can also be constructed with trilinear couplings arising from the scalar potential. When X/Y has a non zero VEV, the mass matrix of neutral scalars has to be diagonalized with two eigenvalues with a large separation. This complication can be avoided with a zero VEV for X and Y . In models with multiple Higgs like doublets, the constraints due to mass splittings become weaker. For example, in MSSM there are five scalar doublets, two from the Higgs superfields and three from lepton superfields which can have the required low mass scalar as well as a 2 TeV resonant scalar[22].

$SU(2)$ triplet R : Similar to the case where R is a singlet, RVX, RXX and RXY type models can be constructed where the triplet particles do not get a VEV. In this case, masses of the zero VEV scalars are obtained as bare masses.

Seven dimensional R : This is an exotic case where a number of multi-charged particles of TeV scale mass arise along with the particle R . In the case of RVX, RXX and RXY ,

the particle X may be a singlet, doublet or 7 dimensional representation of EW symmetry. Additionally, RXX and RXY models can also be constructed with a triplet X, Y . The special case of 7 dimensional X, Y is possible from the perspective of constraints from the ρ parameter. However, a number of light, multi-charged scalars are present in the BSM spectrum which are constrained.

Gauge boson R : When R is a gauge boson, consider the RXX coupling, if X is a gauge field, then we obtain a non minimal extension of SM with two new symmetry groups. This possibility is disfavored as, if X belongs to a $U(1)$ group, RXX coupling does not exist, on the other hand, if X belongs to a non abelian group, anomaly cancellation requires addition of multiple generations of new fermions. RVX, RXX and RXY type models can be constructed when X, Y belong to any of the scalar representations listed above.

C. Some aspects of $2 \rightarrow 3$ topology

In this topology, the final state is such that two of the particles mimic the signal obtained from W/Z bosons and the third particle is not detected with the ATLAS diboson analysis cuts. The reason behind this can be two-fold. First, the third particle can decay into invisible final states and hence will not be detected. But in this case the p_T asymmetry and the invariant mass cut will be able to discard most of these events. This requires the mass of the third hidden particle to be $\lesssim 100$ GeV otherwise large loss in invariant mass or p_T asymmetry would not pass the experimental cuts. Secondly, even if the third particles decays to visible final states, there is a possibility that the third particle is within the fat jet formed by one of the gauge bosons and the decay products of both of them will be seen as a single fat jet. This process is more favourable for light third particle. In the case where, R, X and Y are either singlets or doublets, in addition to the $2 \rightarrow 2$ process, the $2 \rightarrow 3$ process can also, in certain kinematic regimes, provide a signal to the diboson channel. Here we point out that all the models which attempt to explain the diboson excess with a 3 body final state suffer from a set of common constraints. With more number of massive particles in the final state, the phase space suppresses the cross section. The kinematic cuts which ensure that the two fat jets in the final state have a small relative p_T and large separation also add further suppression in this topology. The couplings need to be very large to get a large enough total cross section that after the cuts, so that the required diboson excess is

satisfied.

D. Experimental signatures

Dijet channel at LHC provides a lower bound on the coupling and masses of any BSM particle that couples to quarks or gluons. This constraint would apply to all the proposed R particles and, via the effective couplings with the quarks, to the final state particle X as well. Another interesting channel which has been discussed in detail in a previous section is that of associated production of R with gauge boson. This channel also provides crucial information about the production mechanism of R . In the case where R is produced via a quark initiated process, the total charge of the final state leptons integrated over all the events is positive. However, in the case of gluon initiated process, this number would be 0. This channel provides an independent probe into the RVV type BSM models which can constrain them even with low luminosity ($\sim 5\text{fb}^{-1}$), early results from LHC-13. In particular, models where the particle X decays to $b\bar{b}$ or $\tau^+\tau^-$, the branching fraction to bottom quark should be large and accessible to b-tagged searches at the LHC. Also, the spin of the particle X in the RXX model can be observed through energy fractions of the sub-jets in reconstruction of the W/Z -like particles in the diboson search. Angular correlations of X reconstructed jets can in-turn be used to determine the spin of R once larger data points are available in the high invariant mass region. The branching fraction to tau cannot be large to avoid a significant contribution to the semileptonic channel in the diboson searches where no BSM signal has been observed. In the models where the BSM scalars (X and Y) are $SU(2)$ doublets, presence of light singly charged Higgs put constraint on them. For the particles with 3 and 7 dimensional representations of $SU(2)$, searches for doubly charged Higgs with $T_3 = 0$ limit the mass of such a particle to $M_H^{++} \geq 322$ GeV at 95% CL[37]. Due to this limit, a light neutral scalar X cannot belong to a higher dimensional representation of $SU(2)$ group since the mass splitting among the neutral and charged Higgs requires one neutral scalar to be heavier.

VII. SUMMARY

With the recently observed excess in the resonance searches in diboson channel at the LHC 8 TeV run, we have analyzed the phenomenological signatures of the BSM physics to isolate it in the observed events and provide complimentary signatures for LHC-13 searches. Analysis of the decay channels of diboson process reveals that in the early LHC 13 TeV run, within $\sim 5 \text{ fb}^{-1}$ of data, it would be possible to confirm the existence of a BSM particle which fits the observed excess. In addition, we show that, based on the relative measurements in semileptonic and leptonic channels, as shown in Table III, it will be possible to distinguish between BSM physics contributions to WW , WZ and ZZ channels.

The resonance R proposed to fit the diboson excess may be generated via a quark initiated or a gluon initiated process. The associated production of EW gauge bosons with R can identify the initial state and provide an independent probe into the nature of couplings of R . The particle R will also contribute to the dijet process ($pp \rightarrow R \rightarrow jj$) and the associated dijet process ($pp \rightarrow RV \rightarrow jjV$). When R couples with gluons, the final state $R + j \rightarrow jjj/VVj$ is also possible. Combination of these processes provides a way to constrain all the couplings of R with SM particles.

Since no excess has been observed in the semileptonic channel, we also explore a non-minimal model compatible with this observation. We add an additional particle denoted as X with a mass $\sim 100 \text{ GeV}$ which primarily decay into hadronic final states. This particle can mimic the W/Z signature searched by the experiments and satisfy the observed excess. We discuss the decay modes of X into $\bar{q}q$, gg , $\bar{b}b$ and $\tau^+\tau^-$. A cut on the number of charged tracks (< 30) implies that $X \rightarrow gg$ cannot be the primary decay mode. An analyses of the diboson search with a relaxed cut on number of charged tracks may add the gluon channel increasing the statistical-significance of the excess. A boosted b-tagging or ditau tag would also allow isolation of these decay channels of X .

In addition, we consider a different topology of models with 3 particles in the final state with the decay chain, $pp \rightarrow R \rightarrow VY \rightarrow VVX$ where V is the W/Z boson. The final state particle, X can be invisible or can decay hadronically. The former case successfully fits the diboson excess only for small masses $M_X \approx 10 \text{ GeV}$. For larger values of mass of X , the p_T asymmetry of the two final state gauge bosons becomes too large to pass the experimental cuts. This type of invisible particle can be identified in the boosted diboson fat jets + \cancel{E}_T

process. If X dominantly decays hadronically, it is a part of the boosted fat jet in the final state. Here, we expect to get more sub-jets in one of the fat jets, and may be identifiable by the two mass drops within the reconstructed jet.

In case that LHC-13 indeed finds evidence to support the presence of BSM physics in the EW sector, the possible models can be divided into categories based on their couplings with the qq/gg initial state and EW gauge bosons. We discuss the anatomy of the BSM physics which can explain the diboson excess and categorize the possible s-channel resonances into simplified models and list the couplings. The coupling of R with the EW gauge bosons fixes its SM gauge symmetries to a colorless, SU(2) singlet, doublet, or a 7 dimensional representation.

Finally, our results are applicable to general models which attempt to explain the diboson excess and will enable early detection of the BSM physics at LHC run-II. If the resonance studied here is indeed found at LHC-13, analyses of multiple channels which receive contributions from it will be essential tools to fix the spin, charge and couplings of the BSM particle(s).

VIII. ACKNOWLEDGMENTS

Work of B. Bhattacharjee is supported by Department of Science and Technology, Government of INDIA under the Grant Agreement numbers IFA13-PH-75 (INSPIRE Faculty Award). We thank Sudhir Vempati for many fruitful discussions.

-
- [1] G. Aad *et al.* [ATLAS Collaboration], arXiv:1506.00962 [hep-ex].
 - [2] V. Khachatryan *et al.* [CMS Collaboration], JHEP **1408**, 173 (2014) [arXiv:1405.1994 [hep-ex]].
 - [3] V. Khachatryan *et al.* [CMS Collaboration], Phys. Lett. B **740**, 83 (2015) [arXiv:1407.3476 [hep-ex]].
 - [4] V. Khachatryan *et al.* [CMS Collaboration], JHEP **1408**, 174 (2014) [arXiv:1405.3447 [hep-ex]].
 - [5] G. Aad *et al.* [ATLAS Collaboration], Eur. Phys. J. C **75**, no. 5, 209 (2015) [Eur. Phys. J. C **75**, 370 (2015)] [arXiv:1503.04677 [hep-ex]].

- [6] G. Aad *et al.* [ATLAS Collaboration], *Eur. Phys. J. C* **75**, 69 (2015) [arXiv:1409.6190 [hep-ex]].
- [7] G. Aad *et al.* [ATLAS Collaboration], *Phys. Lett. B* **737**, 223 (2014) [arXiv:1406.4456 [hep-ex]].
- [8] The ATLAS collaboration, ATLAS-CONF-2015-045.
- [9] V. Khachatryan *et al.* [CMS Collaboration], arXiv:1506.01443 [hep-ex].
- [10] CMS Collaboration [CMS Collaboration], CMS-PAS-EXO-14-010.
- [11] G. Aad *et al.* [ATLAS Collaboration], *Eur. Phys. J. C* **75**, no. 6, 263 (2015) [arXiv:1503.08089 [hep-ex]].
- [12] G. Aad *et al.* [ATLAS Collaboration], *Phys. Rev. D* **91**, no. 5, 052007 (2015) [arXiv:1407.1376 [hep-ex]].
- [13] V. Khachatryan *et al.* [CMS Collaboration], *Phys. Rev. D* **91**, no. 5, 052009 (2015) [arXiv:1501.04198 [hep-ex]].
- [14] D. Goncalves, F. Krauss and M. Spannowsky, *Phys. Rev. D* **92**, no. 5, 053010 (2015) [arXiv:1508.04162 [hep-ph]].
- [15] J. Hisano, N. Nagata and Y. Omura, *Phys. Rev. D* **92**, no. 5, 055001 (2015) [arXiv:1506.03931 [hep-ph]]; K. Cheung, W. Y. Keung, P. Y. Tseng and T. C. Yuan, arXiv:1506.06064 [hep-ph]; B. A. Dobrescu and Z. Liu, arXiv:1506.06736 [hep-ph]; A. Alves, A. Berlin, S. Profumo and F. S. Queiroz, *JHEP* **1510**, 076 (2015) [arXiv:1506.06767 [hep-ph]]; Y. Gao, T. Ghosh, K. Sinha and J. H. Yu, *Phys. Rev. D* **92**, no. 5, 055030 (2015) [arXiv:1506.07511 [hep-ph]]; A. Thamm, R. Torre and A. Wulzer, arXiv:1506.08688 [hep-ph]; Q. H. Cao, B. Yan and D. M. Zhang, arXiv:1507.00268 [hep-ph]; J. Brehmer, J. Hewett, J. Kopp, T. Rizzo and J. Tattersall, *JHEP* **1510**, 182 (2015) [arXiv:1507.00013 [hep-ph]]; B. A. Dobrescu and Z. Liu, *JHEP* **1510**, 118 (2015) [arXiv:1507.01923 [hep-ph]]; J. Heeck and S. Patra, *Phys. Rev. Lett.* **115**, no. 12, 121804 (2015) [arXiv:1507.01584 [hep-ph]]; B. C. Allanach, B. Gripaios and D. Sutherland, *Phys. Rev. D* **92**, no. 5, 055003 (2015) [arXiv:1507.01638 [hep-ph]]; T. Abe, T. Kitahara and M. M. Nojiri, arXiv:1507.01681 [hep-ph]; G. Cacciapaglia and M. T. Frandsen, *Phys. Rev. D* **92**, 055035 (2015) [arXiv:1507.00900 [hep-ph]]; T. Abe, R. Nagai, S. Okawa and M. Tanabashi, *Phys. Rev. D* **92** (2015) 5, 055016 doi:10.1103/PhysRevD.92.055016 [arXiv:1507.01185 [hep-ph]]. M. E. Krauss and W. Porod, *Phys. Rev. D* **92**, no. 5, 055019 (2015) [arXiv:1507.04349 [hep-ph]]; P. S. Bhupal Dev and R. N. Mohapatra, *Phys. Rev. Lett.* **115**, no. 18, 181803 (2015)

- [arXiv:1508.02277 [hep-ph]]; S. F. Ge, M. Lindner and S. Patra, *JHEP* **1510**, 077 (2015) [arXiv:1508.07286 [hep-ph]]; F. F. Deppisch, L. Graf, S. Kulkarni, S. Patra, W. Rodejohann, N. Sahu and U. Sarkar, arXiv:1508.05940 [hep-ph]; U. Aydemir, D. Minic, C. Sun and T. Takeuchi, arXiv:1509.01606 [hep-ph]; L. Bian, D. Liu, J. Shu and Y. Zhang, arXiv:1509.02787 [hep-ph]; P. Coloma, B. A. Dobrescu and J. Lopez-Pavon, arXiv:1508.04129 [hep-ph]; T. Bandyopadhyay, B. Brahmachari and A. Raychaudhuri, arXiv:1509.03232 [hep-ph]; R. L. Awasthi, P. S. B. Dev and M. Mitra, arXiv:1509.05387 [hep-ph]; P. Ko and T. Nomura, arXiv:1510.07872 [hep-ph]; J. H. Collins and W. H. Ng, arXiv:1510.08083 [hep-ph]; B. A. Dobrescu and P. J. Fox, arXiv:1511.02148 [hep-ph].
- [16] L. Bian, D. Liu and J. Shu, arXiv:1507.06018 [hep-ph]; K. Lane and L. Prichett, arXiv:1507.07102 [hep-ph]; M. Low, A. Tesi and L. T. Wang, *Phys. Rev. D* **92**, no. 8, 085019 (2015) [arXiv:1507.07557 [hep-ph]]; A. Carmona, A. Delgado, M. Quirs and J. Santiago, *JHEP* **1509**, 186 (2015) [arXiv:1507.01914 [hep-ph]]; C. W. Chiang, H. Fukuda, K. Harigaya, M. Ibe and T. T. Yanagida, arXiv:1507.02483 [hep-ph]; V. Sanz, arXiv:1507.03553 [hep-ph]; C. Niehoff, P. Stangl and D. M. Straub, arXiv:1508.00569 [hep-ph]; C. Niehoff, P. Stangl and D. M. Straub, arXiv:1508.00569 [hep-ph]; H. S. Fukano, S. Matsuzaki, K. Terashi and K. Yamawaki, arXiv:1510.08184 [hep-ph];
- [17] Y. Omura, K. Tobe and K. Tsumura, *Phys. Rev. D* **92**, no. 5, 055015 (2015) [arXiv:1507.05028 [hep-ph]]; D. Aristizabal Sierra, J. Herrero-Garcia, D. Restrepo and A. Vicente, arXiv:1510.03437 [hep-ph]; J. Brehmer, A. Freitas, D. Lopez-Val and T. Plehn, arXiv:1510.03443 [hep-ph]; S. Jung, J. Song and Y. W. Yoon, arXiv:1510.03450 [hep-ph]; Y. Kikuta and Y. Yamamoto, arXiv:1510.05540 [hep-ph]; J. Brehmer, A. Freitas, D. Lopez-Val and T. Plehn, arXiv:1510.03443 [hep-ph]; C. H. Chen and T. Nomura, arXiv:1509.02039 [hep-ph]; S. Zheng, arXiv:1508.06014 [hep-ph]; G. Cacciapaglia, A. Deandrea and M. Hashimoto, *Phys. Rev. Lett.* **115** (2015) 17, 171802 [arXiv:1507.03098 [hep-ph]]; S. Jung, J. Song and Y. W. Yoon, arXiv:1510.03450 [hep-ph]; D. Aristizabal Sierra, J. Herrero-Garcia, D. Restrepo and A. Vicente, arXiv:1510.03437 [hep-ph].
- [18] W. Chao, arXiv:1507.05310 [hep-ph].
- [19] C. H. Chen and T. Nomura, *Phys. Lett. B* **749**, 464 (2015) [arXiv:1507.04431 [hep-ph]].
- [20] L. A. Anchordoqui, I. Antoniadis, H. Goldberg, X. Huang, D. Lust and T. R. Taylor, *Phys. Lett. B* **749**, 484 (2015) [arXiv:1507.05299 [hep-ph]]. A. E. Faraggi and M. Guzzi,

- arXiv:1507.07406 [hep-ph];
- T. Li, J. A. Maxin, V. E. Mayes and D. V. Nanopoulos, arXiv:1509.06821 [hep-ph];
A. E. Faraggi and J. Rizos, arXiv:1510.02663 [hep-ph].
- [21] C. Petersson and R. Torre, arXiv:1508.05632 [hep-ph].
- [22] B. C. Allanach, P. S. B. Dev and K. Sakurai, arXiv:1511.01483 [hep-ph].
- [23] H. S. Fukano, M. Kurachi, S. Matsuzaki, K. Terashi and K. Yamawaki, Phys. Lett. B **750**, 259 (2015) [arXiv:1506.03751 [hep-ph]].
- [24] D. B. Franzosi, M. T. Frandsen and F. Sannino, arXiv:1506.04392 [hep-ph].
- [25] D. Kim, K. Kong, H. M. Lee and S. C. Park, arXiv:1507.06312 [hep-ph]; S. Fichtel and G. von Gersdorff, arXiv:1508.04814 [hep-ph].
- [26] A. Belyaev, N. D. Christensen and A. Pukhov, Comput. Phys. Commun. **184**, 1729 (2013) [arXiv:1207.6082 [hep-ph]].
- [27] T. Sjostrand, S. Mrenna and P. Z. Skands, JHEP **0605**, 026 (2006) [hep-ph/0603175].
- [28] M. Cacciari, G. P. Salam and G. Soyez, Eur. Phys. J. C **72**, 1896 (2012) [arXiv:1111.6097 [hep-ph]].
- [29] CMS Collaboration [CMS Collaboration], CMS-PAS-BTV-13-001.
- [30] J. Gallicchio and M. D. Schwartz, Phys. Rev. Lett. **107**, 172001 (2011) [arXiv:1106.3076 [hep-ph]], A. J. Larkoski, G. P. Salam and J. Thaler, JHEP **1306**, 108 (2013) [arXiv:1305.0007 [hep-ph]]; B. Bhattacharjee, S. Mukhopadhyay, M. M. Nojiri, Y. Sakaki and B. R. Webber, JHEP **1504**, 131 (2015) [arXiv:1501.04794 [hep-ph]]; A. J. Larkoski, I. Moutl and D. Neill, arXiv:1507.03018 [hep-ph].
- [31] S. P. Liew and S. Shirai, arXiv:1507.08273 [hep-ph].
- [32] F. Yu, arXiv:1308.1077 [hep-ph].
- [33] J. A. Aguilar-Saavedra, JHEP **1510**, 099 (2015) [arXiv:1506.06739 [hep-ph]].
- [34] R. Slansky, Phys. Rept. **79**, 1 (1981).
- [35] G. Bhattacharyya, Rept. Prog. Phys. **74**, 026201 (2011) [arXiv:0910.5095 [hep-ph]].
- [36] P. Gambino and M. Misiak, Nucl. Phys. B **611**, 338 (2001) [hep-ph/0104034].
- [37] G. Aad *et al.* [ATLAS Collaboration], Eur. Phys. J. C **72**, 2244 (2012) [arXiv:1210.5070 [hep-ex]].